The Astronomical Journal, 124:2980–2989, 2002 November

MID-INFRARED SPECTROSCOPY OF INFRARED-LUMINOUS GALAXIES WITH SUBARCSECOND RESOLUTION[1]

B. T. Soifer,[2] G. Neugebauer,[3] K. Matthews, and E. Egami[3]
Palomar Observatory, 320-47, California Institute of Technology, Pasadena, CA 91125;
bts@irastro.caltech.edu, gxn@irastro.caltech.edu, kym@caltech.edu, eegami@as.arizona.edu

and

A. J. Weinberger[4]
Department of Physics and Astronomy, UCLA, Los Angeles, CA 90095-1562;
weinberger@dtm.ciw.edu
Received 2002 January 22; accepted 2002 July 18

ABSTRACT

Low spectral resolution ($\Delta\lambda/\lambda \sim 50$) mid-infrared observations with high angular resolution (0.″3–0.″5) using the Long Wavelength Spectrometer on the Keck I Telescope are reported of the nuclei of five highly luminous infrared-bright galaxies. Spectra of eight distinct nuclei, ranging in luminosity from $\sim 10^{11}$ to more than $10^{12}\ L_{\odot}$ have been obtained. Four of the nuclei show the characteristic polycyclic aromatic hydrocarbon (PAH) emission features, i.e., 11.3 μm emission, as well as the 8.6 μm shoulder of the 7.7 μm band. The other nuclei show either weak PAH emission bands or no evidence for these bands. The high spatial resolution of the observations reveals extended emission in the 11.3 μm PAH band associated with several of the compact nuclear sources. When proper account is taken of the diffuse PAH emission, most of the compact sources show little or no directly associated PAH emission. The diffuse PAH emission is extended over spatial scales of 100–500 pc; its presence shows that there is significant circumnuclear UV–optical emission exciting the aromatic bands, most likely associated with circumnuclear starbursts. After the spectra of the nuclear sources are corrected for the spectrum of the diffuse PAH emission, the peak apparent silicate optical depth at 9.7 μm can be as large as 15, corresponding to more than 150 mag of visible light extinction. Because of the large silicate optical depths, mid-infrared spectra are not probing the nature of the true nuclei in the most opaque compact sources.

Key words: galaxies: individual (Arp 220, IRAS 08572+3915, Markarian 273, Markarian 463, VV 114) — infrared radiation — techniques: spectroscopic

1. INTRODUCTION

Submillimeter observations (e.g., Eales et al. 2000; Blain et al. 1999) suggest that ultraluminous infrared galaxies (ULIRGs) at high redshift can account for the cosmic IR background (see Hauser & Dwek 2001). If powered by star formation, these ULIRGs can account for as much star formation as in the galaxies detected in the UV continuum. Alternatively, if the infrared luminosity is attributed to dust-enshrouded active galactic nuclei (AGNs), the cosmic IR background could be measuring the integrated accretion power generated over the history of the universe.

Such observations illustrate the importance of understanding the origin of the luminosity in infrared-bright galaxies. Because these galaxies are by their nature dusty, the normal optical–near-infrared diagnostics break down, since the luminosity sources are obscured by many magnitudes of visual extinction. Attributing the luminosity to dust enshrouded star formation or accretion onto black holes has drastically different consequences for assessing the star formation history of the universe.

Recent spectroscopic observations from the *Infrared Space Observatory* (*ISO*) have suggested that spectroscopic diagnostics of the underlying power sources do exist within the mid-infrared. Genzel et al. (1998) suggested that there is a correspondence between the presence of strong aromatic features (polycyclic aromatic hydrocarbons, commonly referred to as PAHs) at 6.2, 7.7, 8.6, and 11.3 μm and other diagnostics of stellar ionizing radiation from young massive stars, while weak or nonexistent aromatic features are associated with infrared galaxies whose luminosity is generated via AGNs.

The *ISO* observations were hampered by the large observing beams, which included nearly all the infrared light from the galaxies, thereby combining both nuclear and circumnuclear emission. In Seyfert galaxies such as NGC 1068 and NGC 7469 (see Myer & Scoville 1987; Wilson et al. 1991), large observing beams include both a nuclear AGN and a circumnuclear starburst, so that the integrated spectrum is a combination of radiation generated in multiple regions with widely varying excitation conditions.

Ground-based, airborne, and space-based observations, e.g., Gillett et al. (1975b), Willner et al. (1977), Helou et al. (2000), and Sturm et al. (2000), have demonstrated that the full suite of PAH features is readily seen in many galaxies.

[1] Based on observations obtained at the W. M. Keck Observatory, which is operated as a scientific partnership among the California Institute of Technology, the University of California, and the National Aeronautics and Space Administration.

[2] Also at *SIRTF* Science Center, 220-6, California Institute of Technology, Pasadena, CA 91125.

[3] Current address: Steward Observatory, University of Arizona, 933 North Cherry Avenue, Tucson, AZ 85721.

[4] Current address: Department of Terrestrial Magnetism, Carnegie Institution of Washington, 5241 Broad Branch Road, NW, Washington, DC 20015-1305.

Indeed, as shown by Genzel et al. (1998), Lutz et al. (1998), Rigopoulou et al. (1999), and Tran et al. (2001), these bands can dominate the mid-infrared spectra of ULIRGs. The 11.3 μm feature is readily detectable, having a line-to-continuum ratio roughly half that of the 7.7 μm band in nearby galaxies such as M82 (Gillett et al.; Sturm et al.). Thus, the detection of PAH emission via the 11.3 μm band should be nearly equivalent to using the broader 7.7 μm complex of features. The presence of the 9.7 μm silicate feature, which can produce strong absorption over the entire 8–13 μm region, complicates the interpretation of mid-infrared spectra. Silicate absorption has been shown to be quite strong in some galaxy spectra (Roche et al. 1991).

The upcoming launch of *SIRTF*, with its capability of studying the spectra of ULIRGs to redshifts substantially greater than 1, highlights the need to develop infrared diagnostics of the luminosity in dusty luminous galaxies. We have obtained low spectral resolution ($\lambda/\Delta\lambda \sim 50$) mid-infrared observations from 8 to 12.5 μm of a sample of infrared-luminous galaxies with 0.″3–0.″5 spatial resolution using the Long Wavelength Spectrometer (LWS) on the Keck I telescope. With this spatial resolution we have been able to isolate individual compact sources that are emitting copiously in the infrared and are our best local examples of ULIRGs.

Spectroscopy of some of the sources observed here has been reported by Smith, Aitken, & Roche (1989), Roche et al. (1991), and Dudley (1999). The data reported here are obtained with substantially higher spatial resolution that has allowed us to resolve the separate nuclei in the multiple nuclei sources, as well as to explicitly detect spatially extended PAH emission associated with the nuclei.

2. SAMPLE

The objects observed were selected to be high-luminosity galaxies that are bright at 12 μm. VV 114, Mrk 273, IRAS 08572+3915, and Arp 220 were all selected from the IRAS Bright Galaxy Sample (Soifer et al. 1987), while Mrk 463E is included in the Ultraluminous Warm Galaxy Sample (Sanders et al. 1988b). The total infrared luminosities of the systems range from $4 \times 10^{11}\ L_\odot$ for VV 114 (Soifer et al.) to $1.5 \times 10^{12}\ L_\odot$ for Arp 220 (Sanders et al. 1988a). Mid-infrared imaging with resolution of 0.″3–0.″5 has been previously reported for Arp 220, Mrk 273, IRAS 08572+3915, and VV 114 (Soifer et al. 1999, 2000, 2001). In VV 114, Arp 220, and Mrk 273, two compact sources were seen at 12.5 μm, while in IRAS 08572+3915 a single unresolved source was detected that contains nearly all the bolometric luminosity of the source. No mid-infrared imaging of Mrk 463 has been reported in the literature; as shown below, the present observations show a compact core, which emits essentially all the mid-infrared luminosity of the galaxy. Table 1 lists the basic properties of the sources that were observed.

TABLE 1

BASIC PROPERTIES OF OBSERVED GALAXIES

Name	z	$\log \frac{L}{L_{\rm bol}(L_\odot)}$	Spectrum OPT	Linear Scale (kpc/arcsec)
VV 114=IC 1623.....	0.020	11.62	H II	400
IRAS 08572+3915.....	0.058	12.10	LINER	1200
Mrk 463E.....	0.050	12.03	Seyfert 1	1000
Mrk 273	0.037	12.13	Seyfert	800
Arp 220.....	0.018	12.17	LINER	360

3. OBSERVATIONS AND DATA REDUCTION

The observations were made using the low-resolution spectroscopic mode of the LWS (Jones & Puetter 1993) at the f/25 forward Cassegrain focus of the Keck I 10 m telescope. Briefly, LWS includes a grating spectrometer, which contains a 128 × 128 pixel Si:As array. The spectral dispersion is 0.0375 μm pixel^{-1}, and the spatial scale is 0.08″ pixel^{-1}. For the present spectroscopy, a filter with bandpass from 8.1 to 13.0 μm was used for order selection; 128 × 95 pixels (dispersion × cross dispersion) were unvignetted, so a wavelength coverage of 4.8 μm was available over a 7.″6 slit length.

The present observations were obtained in 2000 May, 2000 September, and 2000 December. A log of the observations is presented in Table 2. The observations were made at air masses between 1.1 and 1.5. The atmospheric absorption in the observed spectra was monitored by observing HR=BS 5340 in 2000 May and BS 8775 in 2000 September and 2000 December at similar air masses. For each source an image at 12.5 or 11.7 μm was obtained using the imaging mode of the LWS before spectra were taken as part of the procedure of setting up the target for spectroscopic observations. Observations of stars indicated the seeing had an FWHM between 0.″3 and 0.″4. The FWHM and the total on-source integration times for the objects observed are listed in Table 2.

The observations used chopping at a frequency of ~1.7 Hz and nodding of the telescope every ~30 s to suppress sky emission. The telescope was nodded in the same direction as the chopping, and the nodding amplitude was the same as the chopping amplitude given in Table 2. The chopping or nod direction was set parallel to the slit so that, if the source structure allowed a sufficiently small chopping amplitude, three dispersed images of the objects were on the array. Observations were divided into runs of ~6 minutes each. During the observations of the objects, the telescope tracking was controlled using an offset guider with a visible guide star.

For all these observations the slit was 6 pixels (0.″48) wide, corresponding to a spectral resolution of 0.22 μm or $\lambda/\Delta\lambda \sim 50$ for a source uniformly filling the slit. Because the seeing was typically less than the slit width, the spectral resolution was set by the image size, not by the slit width. The seeing disk is close to the diffraction limit, which results in a variable image size; hence the spectral resolution varies with wavelength. In general, the slit position angle on the sky was determined by the location of an appropriately bright offset guide star. This limited the observations to only one infrared component at a time in VV 114 and Mrk 273, even though there were two distinct source components. In the case of Arp 220 a guide star could be used that allowed the slit to be oriented such that both nuclei, separated by ~1″ (Soifer et al. 1999), could be observed in a single spectrum.

The spectra were reduced by first combining the individual images to subtract the sky contribution. The resultant images were then co-added after appropriately shifting the images (1) parallel to the slit to co-add the rows containing the object and (2) in the dispersion direction to align the ozone emission present in the raw un–sky-subtracted frames. One-dimensional spectra were obtained by extract-

TABLE 2
OBSERVING LOG

Object	Date (2000)	FWHM[a] (arcsec)	Obs. Time[b] (s)	Chop. Amp. (arcsec)	P.A.[c] (deg)	Averaging Range[d] (μm)	Averaging Width[e] (μm)
VV 114E$_{SW}$	Sep	0.30	1200	5.0	69	8.91–9.64	0.26
VV 114E$_{NE}$	Dec	0.35	400	10.0	166	8.98–10.34	0.26
IRAS 08572+3915	Dec	0.42	200	10.0	157	9.37–9.72	0.26
Mrk 463E	May	0.36	800	3.0	61	...	...
Mrk 273NE	May	0.35	2600	3.0	83	8.98–10.79	0.26
Mrk 273SW	May	0.39	4800	3.0	83	...	...
Arp 220W	May	0.30	3000	3.0	92	9.11–10.29	0.19
Arp 220E	May	0.30	3000	3.0	92	9.00–10.11	0.34

[a] FWHM of nearby PSF star.
[b] Includes time of negative images on array; see text.
[c] Position angle of slit measured east of north.
[d] Wavelength range in rest frame over which additional running average greater than 0.11 μm was taken; see text.
[e] Wavelength width of additional running average greater than 0.11 μm; see text.

ing five rows (0″.40) centered on the maximum emission and subtracting from this the spectrum of the night sky extracted in the two-dimensional spectral image well away from the object. To increase the signal-to-noise ratios, 3 pixels (half the slit width) throughout the wavelength range of the spectra were averaged in a running average. Many of the spectra showed a deep absorption band and consequently had locally extremely low signal-to-noise ratios. For some of these spectra a running average of several more pixels over the wavelength range of low signal was taken, reducing the spectral resolution but increasing the signal-to-noise ratio. The resultant spectral resolution is indicated in Table 2. The noise per pixel at each wavelength was calculated from the "sky" well away from the object.

Atmospheric and instrumental features, most notably the deep atmospheric ozone absorption at 9.6 μm, were removed by dividing the object spectrum by the spectrum of BS 5340 and multiplying by a blackbody spectrum at the star's effective temperature. Since the stellar image was generally smaller than the slit width, the star set both the spectral resolution and wavelength scale of the spectrum and was often at a different wavelength than that of the associated galaxy spectrum, as evidenced by sharp discontinuities at the edges of the ozone absorption band. After extensive experimentation, it was found better to use an average spectrum of 15 observations of BS 5340 than a single spectrum of a nearby (in time) stellar observation.

The wavelengths of the stellar spectrum were established by comparing the observed stellar spectrum of BS 5340 with models of the earth's transmission over this wavelength range calculated by Lord (1992). The final wavelength solution for each object was refined, within the bounds set by the ozone emission, by identifying different astrophysical or terrestrial atmosphere features in each object. In VV 114E$_{NE}$, Mrk 273N, and Arp 220 it was possible to use the emission of the PAH band at 11.25 μm (hereafter referred to as the 11.3 μm feature) in the rest frame to set the wavelengths. In Mrk 463E the continuum was strong enough that the atmospheric ozone absorption was detectable in individual spectra and was used to establish the wavelength scale. For the remaining three objects, an attempt was made to match the deep atmospheric absorption at 9.6 μm before dividing by the stellar spectrum.

4. RESULTS

The mid-infrared spectra of the galaxy nuclei are presented in Figure 1. The individual spectra are described in the following sections.

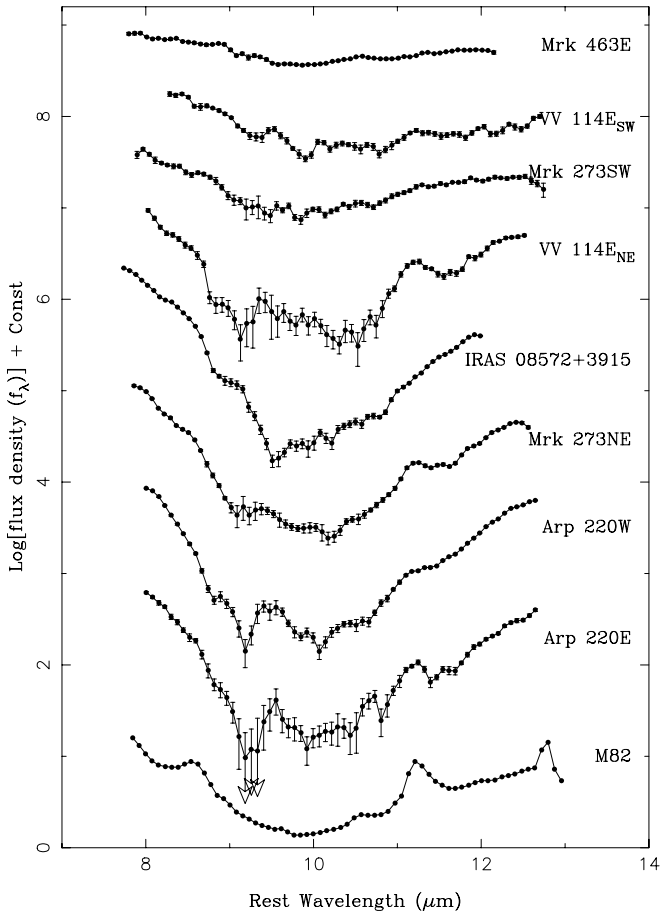

FIG. 1.—Mid-infrared spectra of the separate nuclei plotted vs. rest wavelength. The logarithms of the flux densities per wavelength interval in relative units are plotted. Arrows indicate limits. The spectrum of M82, binned to the spectral resolution of the present data, is taken from Sturm et al. (2000).

4.1. *VV 114*

The structure of VV 114 is dominated at infrared wavelengths by two compact sources (Knop et al. 1994; Doyon et al. 1995; Soifer et al. 2001), both within the highly obscured eastern component of the source, referred to by Soifer et al. as VV 114E$_{NE}$ and VV 114E$_{SW}$. Imaging at 2.2 μm of VV 114E with NICMOS on the *Hubble Space Telescope* (Scoville et al. 2000) showed that VV 114E$_{NE}$ is slightly extended while VV 114E$_{SW}$ is unresolved. Mid-infrared photometry of these sources (Soifer et al. 2001) reveals a deeper depression in the mid-infrared spectral energy distribution in the brighter northeast component.

Figure 1 shows the spectra of VV 114E$_{NE}$ and VV 114E$_{SW}$. The two peaks are separated by 1.″8 at 12.5 μm (Soifer et al. 2001). With seeing of 0.″4 the slit width of 0.″5 isolates the separate peaks. The spectra show that indeed the 10 μm depression of VV 114E$_{NE}$ is significantly deeper than that in VV 114E$_{SW}$. The spectrum of VV 114E$_{NE}$ shows the characteristic feature of aromatics, i.e., a peak at 11.3 μm, a shoulder at 8.6 μm, and the continued rise to the shortest observed wavelengths. The minimum flux in the spectrum is at about 10.2 μm, consistent with the aromatic spectrum of normal galaxies as seen by *ISO* (Helou et al. 2000).

By comparison the spectrum of VV 114E$_{SW}$ shows a shallower rise to longer wavelengths and a weak 11.3 μm feature. The equivalent width of the 11.3 μm feature in VV 114E$_{SW}$ is less than half that in VV 114E$_{NE}$. In addition, the minimum of the flux appears to occur at shorter wavelengths, closer to 9.8 μm in the rest frame of the galaxy (although this might be due to a slight mismatch in the correction for the terrestrial ozone absorption at 9.6 μm.)

4.2. *IRAS 08572+3915*

IRAS 08572+3915 was found by Soifer et al. (2000) to be a single very compact source (<0.″3) at 12.5 μm that contained nearly all the mid-infrared luminosity detected in the $\sim$1′ IRAS beam measurements. The mid-infrared spectrum of IRAS 08572+3915 is shown in Figure 1. The spectrum shows a strong depression at 10 μm, much greater than expected from the photometry reported by Soifer et al. but consistent with that seen by Dudley & Wynn-Williams (1997). This is a result of the redshift of this object, which puts the deep depression outside the sampling of the photometric filters used by Soifer et al.

There is no evidence for PAH features in the spectrum. Rather the spectrum is characteristic of strong absorption by cold silicate dust overlying a warmer background source (e.g., Gillett et al. 1975a), showing a deep minimum at 9.7 μm.

4.3. *Mrk 273*

Soifer et al. (2000) showed that this galaxy is dominated by two compact sources separated by 1″ at mid-infrared wavelengths. Mrk 273NE is slightly extended, mostly in the east-west direction in the NICMOS 2.2 μm image of Scoville et al. (2000), while Mrk 273SW is unresolved in the same NICMOS 2.2 μm image. Soifer et al. showed that the northern source is generally brighter in the mid-infrared, but with a stronger depression at 10 μm.

The mid-infrared spectra of the separate nuclei of Mrk 273 are shown in Figure 1. With seeing of $\sim$0.″3 the 0.″5 slit adequately separates the spectra of the two nuclei. Mrk 273NE shows a broad depression centered shortward of 10 μm, rising steeply to shorter and longer wavelengths. The spectrum shows a clear peak at 11.3 μm and shoulder at 8.6 μm showing the presence of the aromatic PAH features.

The spectrum of Mrk 273SW is significantly different from that of Mrk 273NE, i.e., much less depression at 10 μm and little evidence for an 11.3 μm feature. The rise in flux to shorter wavelengths coincides with that seen in the northern source. The flattening at $\lambda < 8.6$ μm is suggestive of PAH emission.

4.4. *Mrk 463E*

Mrk 463E was found by Sanders et al. (1988b) to be a high-luminosity galaxy with a "warm" mid-infrared color, i.e., larger 25/60 μm flux density ratio than most ULIRGs in the IRAS Bright Galaxy Sample (Soifer et al. 1987; Sanders et al. 1988a). The optical spectroscopic classification of Mrk 463E is that of a Seyfert galaxy (Miller & Goodrich 1990).

Imaging at 12.5 μm done in conjunction with the mid-infrared spectroscopy shows Mrk 463E to be compact, with a source of angular diameter less than 0.″5, or 500 pc for a redshift of $z = 0.05$, containing all the 12 μm flux measured by IRAS. The mid-infrared spectrum is shown in Figure 1. The spectrum shows a drop from 8.0 to 9.6 μm, a minimum at $\sim$10.0 μm, and then a slightly rising continuum to longer wavelengths. There is structure in the spectrum at about 9.2 μm, which is most likely associated with imperfectly corrected ozone absorption in the observations. There is a peak at 10.55 μm and no evidence for peaks at 8.6 or 11.3 μm. The peak at 10.55 μm could represent [S IV] emission, which is strong in *ISO* spectra of comparable sources (Sturm et al. 1999; Lutz et al. 2000).

4.5. *Arp 220*

Arp 220 is the closest ULIRG (Soifer et al. 1984; Sanders et al. 1988a), at redshift $z = 0.018$. The two nuclei seen at 12.5 μm (Soifer et al. 1999) are separated by 1″ or 360 pc. The slit position angle was 92° so that both nuclei were on the slit at the same time. The seeing was $\sim$0.″3 for the observations, so that the spectra of the nuclei are well separated.

The spectra of the separate nuclei are shown in Figure 1. The spectra of both nuclei show strong minima at $\sim$10 μm with roughly the same depression compared with the flux density at 8 μm. The spectra of the nuclei are quite similar, the fainter eastern component shows somewhat stronger PAH emission, with a clear peak at 11.3 μm and a shoulder at 8.6 μm. In the brighter western source the PAH features are present but not as prominent.

4.6. *Diffuse PAH Emission*

The continuum sources are spatially compact, consistent with the sizes measured in previous imaging observations (Soifer et al. 1999, 2000, 2001). In addition to the compact continuum structure, there is extended emission in the 11.3 μm PAH emission feature in some galaxy nuclei in this sample. In the three sources in which this feature is prominent—VV 114E$_{NE}$, Mrk 273NE, and Arp 220—the PAH emission is clearly extended. This is revealed in the two-dimensional spectra of these sources shown in Figure 2.

Figure 2 (*top*) displays a gray-scale image of the two-dimensional spectrum in the region of the 11.3 μm PAH feature in Arp 220 with a contour plot of the intensity. The

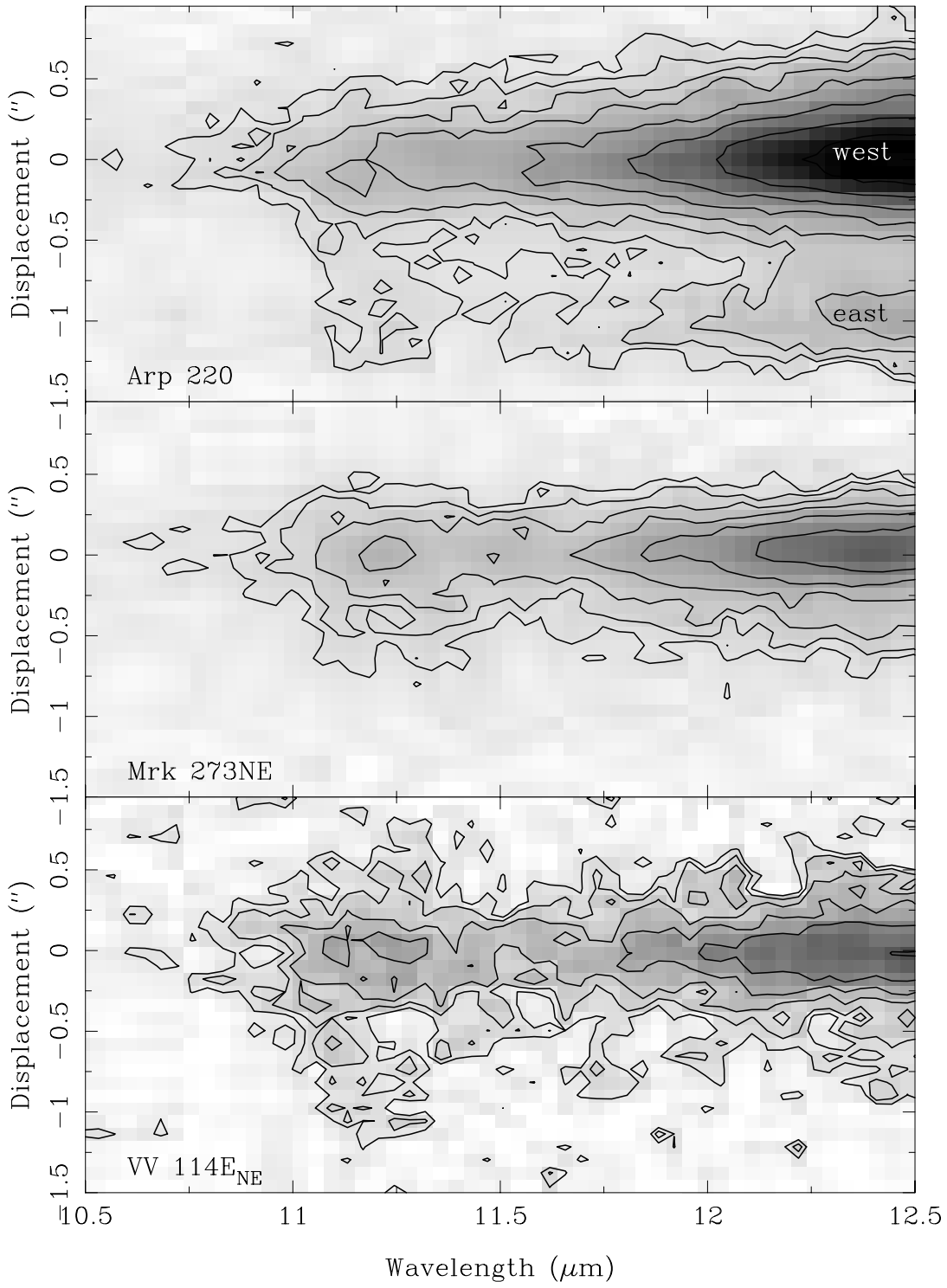

FIG. 2.—Contour plots overlaid on gray-scale plots of the two-dimensional spectra of Arp 220 (*top*), Mrk 273NE (*middle*), and VV 114E$_{NE}$ (*bottom*). In all cases, rest wavelength is plotted along the abscissa, and spatial dimension is along the ordinate. In each case the strong continuum source is readily seen, while at the wavelength of the PAH emission (11.25 μm) extended emission along the spatial dimension is also seen. Slight wavelength shifts appear as a result of the shifts of the centroid of the PAH-band emission (in the *x*-spatial dimension) within the slit along the *y*-spatial dimension. In Arp 220 the PAH emission is seen between the two continuum sources; in VV 114E$_{NE}$, PAH emission is seen on both sides of the continuum source, while in Mrk 273NE the PAH emission extends to only one side of the continuum source.

continuum emission from the two compact sources in Arp 220 is clearly seen along the spectral dimension, while at 11.3 μm a band is seen bridging the 1.″0 (360 pc) gap between the two continuum sources. There is weak PAH emission extending beyond the eastern source (see below). In Figure 2 (*middle*), spatially extended PAH emission is seen extending to one side of the continuum source in Mrk 273NE by about 0.″7 (500 pc).

In VV 114E$_{NE}$ (Fig. 2, *bottom*) there is clear 11.3 μm emission extending in the spatial domain in both directions from

the continuum source. The PAH emission extends ~1″.3 (500 pc) south and 0″.7 (300 pc) north of the continuum source. An artifact of the observations, which is most clearly seen in the contour plot or gray scale of Figure 2 (*bottom*), is the apparent shift of the wavelength of the PAH feature along the spatial dimension. The shift is probably a result of the seeing disk being small compared with the slit width (0″.5), so that shifts in the centroid of the emission within the slit translate in the spectra to apparent shifts in the wavelength along the slit.

To show the spatial distribution of the PAH emission in Arp 220 in more detail, we have constructed a PAH-only spectral image by subtracting a modeled continuum emission. The results are shown in Figure 3. The spatial profile of the continuum was derived by summing the two-dimensional spectral image (Fig. 3*a*) over wavelengths longward of 12 μm, where the continuum is strong and there is no strong emission line. Then, the continuum spectrum was constructed in two stages. First, seven rows (i.e., pixels in the spatial direction) centered on the maximum emission of the western nucleus were summed to create an average spectrum of the western source. Second, the PAH-contaminated spectral regions were masked, and a fifth-order polynomial was fitted to the average spectrum to produce a one-dimensional pure continuum spectrum. A two-dimensional continuum spectral image was then created by replicating the spatial profile in the wavelength direction with an amplitude determined by the one-dimensional continuum fit.

Figure 3*b* shows the continuum-subtracted PAH-only spectral image. It clearly indicates the diffuse nature of the PAH emission. It can also be seen that the peak of the PAH emission is slightly displaced toward the eastern nucleus.

Figure 3*c* compares the spatial distribution of the continuum and PAH emission. To produce these profiles, the flux over 0.187 μm (five columns) centered on the peak of the PAH emission was summed along the wavelength direction in the PAH-only image (Fig. 3*b*) and the modeled continuum image. This shows a striking difference between the two components. Unlike the double-peaked continuum emission, the PAH emission has a single peak ~0″.25 east of the western nucleus, and is nearly uniformly distributed from this peak toward the eastern nucleus. The PAH emission drops markedly at the center of the western nucleus.

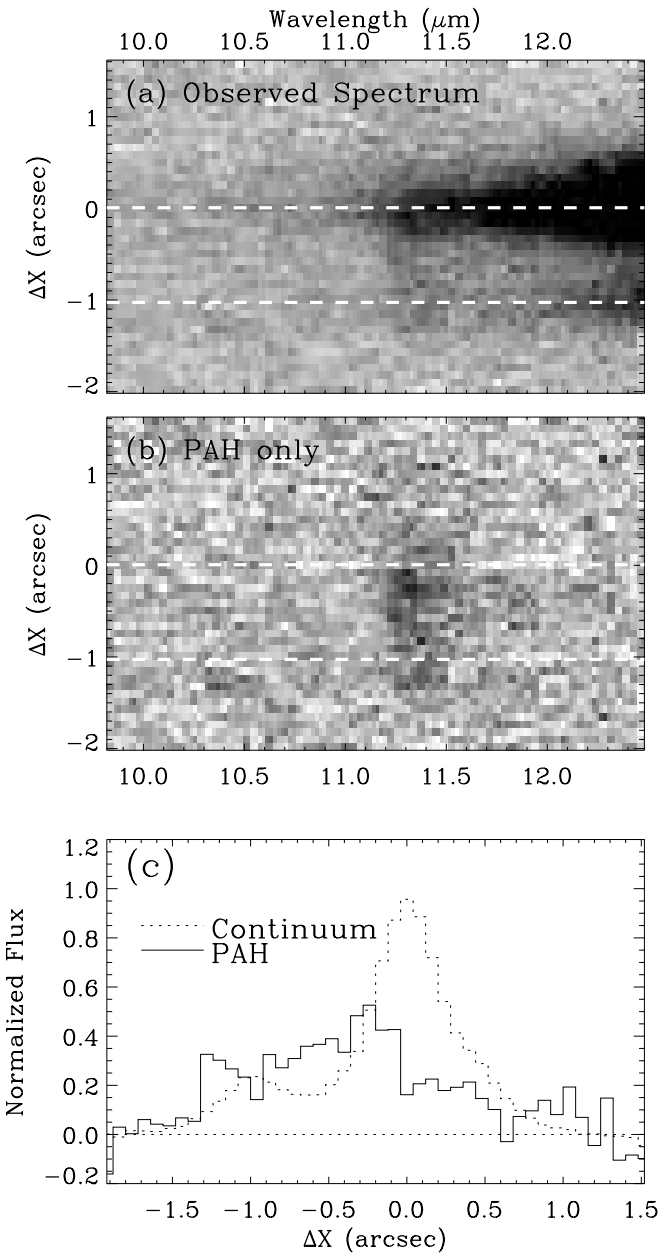

FIG. 3.—Spatial distribution of the 11.3 μm PAH feature in Arp 220. (*a*) Observed two-dimensional spectrum, reproduced from Fig. 2 (*top*). (*b*) Continuum-subtracted two-dimensional spectrum showing only the PAH band. The details of how the continuum was removed are described in the text. (*c*) One-dimensional slice of the spatial distribution of the PAH band (from *b*) and the continuum.

5. DISCUSSION

The spectra presented in Figure 1 show a variety of shapes and features but are quite similar to those seen previously in lower spatial resolution observations (see Roche et al. 1991; Dudley 1999). The overall spectra are a combination of a smooth featureless continuum, absorption due to intervening cold silicate material, and PAH emission features such as seen in the nearby starburst galaxy M82 (see Gillett et al. 1975b; Willner et al. 1977; Roche et al. 1991; Dudley 1999; Sturm et al. 2000). In addition, the high spatial resolution of the spectra, seen in Figure 2, resolves the spectra of the individual nuclei and reveals the extended nature of the PAH emission as compared with the compact continuum sources. The substantially higher spatial resolution (0″.3–0″.5) of the present observations over previous observations permits the separation of the spectra at different spatial locations. In VV 114E_{SW} there is a hint of extended PAH emission in the two-dimensional spectrum, but excess pattern noise in the spectrum precludes determining with any confidence its contribution in the extracted spectrum. In IRAS 08572+3915, Mrk 273SW, and Mrk 463E there is no evidence for PAH emission in the spectrum of the compact source or in the two-dimensional spectrum from which it was extracted.

5.1. *Spectra of the Compact Sources*

The spectra of Arp 220 E, Arp 220 W, VV 114E_{NE}, and Mrk 273NE, corrected for the extended PAH emission, are shown in Figure 4. To correct for the extended PAH emission, the strength of the PAH emission adjacent to the

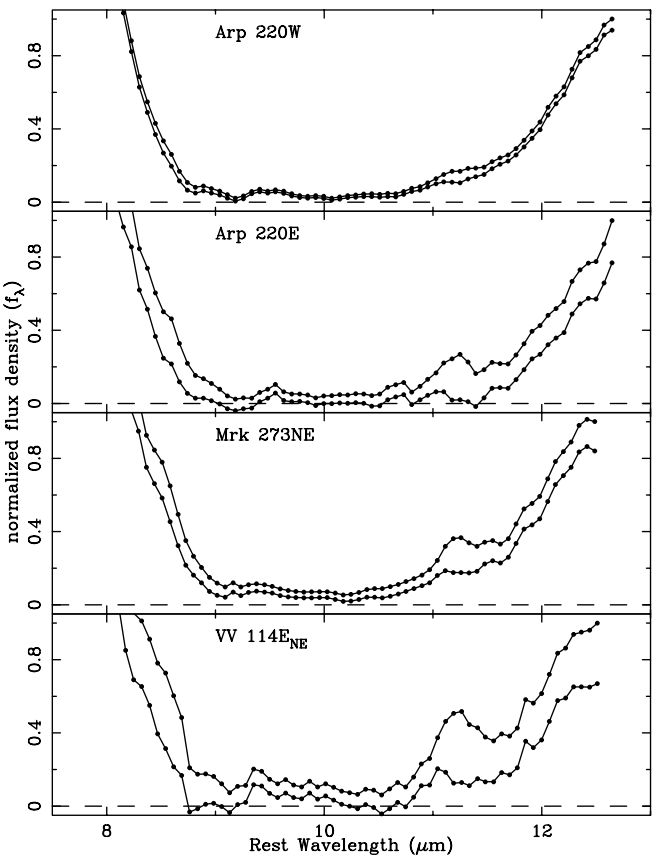

FIG. 4.—Mid-infrared spectra of the nuclei plotted vs. rest wavelength and corrected for the strength of the extended PAH emission as displayed in Fig. 2. The correction was applied by normalizing the spectrum of M82 (Sturm et al. 2000) to the strength of the PAH band adjoining the continuum source and subtracting this spectrum from the corresponding spectrum of Fig. 1; see the text. In each panel the top line is the spectrum from Fig. 1; the bottom line is the spectrum corrected for the overlying extended PAH emission.

compact source was measured in the two-dimensional spectrum, and a spectrum of M82, normalized to this measured PAH strength, was subtracted from the spectrum of the continuum source of Figure 1.

A substantial uncertainty exists in the spectrum of the diffuse emission that is subtracted from the compact sources. We *assume* that this spectrum is universal and like that of M82. Because of the bright compact sources and the faint diffuse emission except in the 11.3 μm PAH band, we could measure the 11.3 μm PAH strength only off the nuclei. We could not independently determine the full spectrum off the nuclei. While the smoothness of the resulting spectra as displayed in Figure 4 suggests the basic validity of our procedure, the potential variation of PAH-to-continuum ratios (e.g., Tran et al. 2001) led to a substantial uncertainty.

Sturm et al. (2000) argue that the mid-infrared spectrum of M82 suffers negligible extinction ($A_V < 5$ mag), based, among other arguments, on model fitting of its spectrum to the observed spectrum of the reflection nebula NGC 7023. However, Willner et al. (1977) estimated the extinction to the infrared continuum in M82 to be $A_V \sim 25$ mag from the measured ratio of the Brα and Brγ emission lines at 2.16 and 4.05 μm. If this latter determination of the extinction applies to the PAH-emitting region, then presumably the M82 spectrum suffers a corresponding silicate absorption of $\tau_{9.7\ \mu m} \sim 2$ in the observed spectrum. The effect of larger extinction on the 10 μm spectrum of M82 is illustrated in Rigopoulou et al. (1999). Increasing the silicate absorption over that of M82 in the subtracted spectrum would have the effect of significantly reducing the 9–11 μm continuum that is subtracted from the observed spectrum, compared with the 11.3 μm strength. In turn, this would decrease the inferred silicate absorption in the continuum sources, by preserving a detectable continuum from 9 to 11 μm.

In Figure 1, VV 114E$_{NE}$ is the source with the strongest PAH emission. As seen in Figure 4, after the extended PAH emission is subtracted from the initial spectrum, little flux remains from 9 to 11 μm. There is a peak close to 11 μm that may be residual PAH emission. The residual continuum is consistent with zero flux in the wavelength range from 9 to 11 μm, suggesting that most of the apparent continuum over these wavelengths in the spectrum of Figure 1 is due to an extended overlying PAH spectrum. The compact continuum source apparently suffers strong absorption by intervening cold silicate material.

In Mrk 273NE a significant PAH feature is seen in Figure 1. Figure 4 shows a weak PAH shoulder feature remaining after subtraction of the extended PAH emission, suggesting that there is a residual PAH band associated with the compact source. This is consistent with the observation of continuum detected in the subtracted spectrum over the entire 9–11 μm range.

In Arp 220E the spectrum of Figure 1 shows a distinct PAH emission peak at 11.3 μm. When the diffuse PAH emission is subtracted from the observed spectrum, there is no evidence for residual PAH emission in the compact source, and the continuum becomes consistent with zero flux from 8.8 to 11.5 μm (Fig. 4). In Arp 220W, where the spectrum of Figure 1 shows a shoulder of PAH emission on a steeply rising continuum, after subtraction of the diffuse PAH emission a weak shoulder remains at 11.3 μm, as does a measurable continuum in the 9–11 μm band.

The spectra of Figure 4 show that the underlying compact sources suffer substantially greater foreground absorption at $\sim$10 μm than would be inferred from the spectra of Figure 1. Smith et al. (1989) have attempted to correct the 10 μm absorption apparent in the spectrum of Arp 220 for overlying PAH emission and derive a peak optical depth of $\tau_{9.7\ \mu m} > 5$, which implies $A_V > 50$ mag. The spectra shown in Figure 4 suggest even greater absorption in the depth of the silicate band. From the spectra of Figure 4 we infer peak optical depths $\tau_{9.7\ \mu m}$ (see below) in the range 8–15, which correspond to optical extinctions A_V of 80–150 mag.

5.2. *Detailed Comparison with ISO Results for Arp 220*

Because it is the closest ULIRG, the results presented here for Arp 220 warrant special discussion. A major finding from these observations is that the two nuclei in Arp 220 are not luminous sources of PAH emission. As seen in Figures 2 and 3, most of the PAH emission in Arp 220 originates in the off-nuclear regions, and a significant fraction actually comes from the region between the two nuclei. Furthermore, the PAH emission drops significantly near the center of the western nucleus, which dominates the mid-infrared continuum luminosity.

The region producing the PAH emission is clearly distinct from the compact sources producing the bulk of the mid-

infrared luminosity and most likely the far-infrared luminosity as well. This argues that the extinction toward the PAH-emitting regions is not likely to be as large as that inferred from the *ISO* data. If the extinction toward the PAH-emitting region were as large as previously suggested (i.e., 50 mag more than to the corresponding regions in M82), star-forming regions directly associated with the PAH-emitting regions would make a dominant contribution to the total continuum luminosity, which is apparently not the case, as seen in Figures 2 and 3*c*. This is in contrast to the picture developed from the *ISO* data, which suggests that the strong PAH emission seen in ULIRGs directly traces star formation that dominates the luminosity output in these galaxies (Genzel et al. 1998; Lutz et al. 1998; Rigopoulou et al. 1999; Tran et al. 2001).

The peak of the PAH emission, $\sim 0\farcs25$ east of the western nucleus, corresponds to the peak of the warm molecular hydrogen detected by Larkin et al. (1995). This suggests that the exciting source of the molecular hydrogen may also be responsible for the PAH emission.

5.3. *Compact Nuclei and the Diffuse PAH Emission*

The excitation mechanism for PAH emission is generally believed to be single UV–optical photon heating of aromatic molecules (see e.g., Sellgren 1984; Draine & Anderson 1985; Leger, D'Hendecourt, & Defourneau 1989). The presence of substantial diffuse PAH emission associated with the luminous compact sources shows that there is a significant optical–UV photon intensity associated with the outer parts of the sources. The spectra of the underlying compact sources show large 10 μm optical depths. Based on the interstellar extinction curve (e.g., Mathis 1990; Li & Draine 2001), this corresponds to an order of magnitude greater extinction in the visible and a factor of $\sim$40 greater optical depth in the UV.

To roughly estimate the silicate optical depths for the sources we assumed an underlying continuum that is constant (in f_λ) and matched the apparent continuum with a silicate absorption profile as a function of wavelength from Gillett et al. (1975a). In the case of the most heavily absorbed sources, where the continuum was not detected from 9 to 11 μm, we matched the observed continuum slope, corrected for PAH emission in Figure 4, between 12 and 12.5 μm (rest frame), and extrapolated the inferred optical depth to the peak optical depth at 9.7 μm. Because of the uncertainties in the shape of the continuum and the simple technique employed for estimating $\tau_{9.7\ \mu\mathrm{m}}$ these are crude estimates of the silicate optical depth.

The range of silicate optical depths and corresponding A_V in these sources is quite large. With $\tau_{9.7\ \mu\mathrm{m}} \sim 1$ in Mrk 463E, A_V is $\sim$10 mag, while in the most highly obscured sources, such as Arp 220E, the silicate optical depths are as great as $\sim$15, corresponding to $A_V \sim$ 150 mag. Given the much higher spatial resolution of the present observations, it is not surprising that the extinction derived for the highly embedded sources in Arp 220 are larger by a factor of 2–3 than those determined from large-beam *ISO* spectroscopic studies (e.g., Sturm et al. 1996). The extinction to the continuum sources in Arp 220 is roughly an order of magnitude greater than that derived by Larkin et al. (1995) from the Pβ/Brγ line ratios in these same nuclei. It is common to find increased extinction determined at wavelengths that probe deeper into the regions; this suggests that we are still probing to $\tau \sim 1$ at the observed wavelengths.

The extinctions derived here are so large that it is most unlikely that the UV–optical photons that excite the extended PAH emission arise internally in the compact sources. Much more likely is a large UV–optical radiation field generated because of hot young stars in the periphery of the compact sources. The circumnuclear regions indeed have internal dust that implies extinction of the ionizing starlight, but not in the huge columns implied from the large silicate optical depths derived above. The presence of such a circumnuclear environment is not surprising, since powerful circumnuclear starbursts have been suggested for Arp 220 and Mrk 273 from the distribution of CO gas (Sakamoto et al. 1999; Downs & Solomon 1998).

We can crudely estimate the total luminosity associated with the diffuse PAH emission by determining the total flux in the diffuse 11.3 μm PAH band and applying a bolometric correction based on an assumed ratio of the PAH band to total luminosity. If we assume that M82 has a typical PAH-to-bolometric luminosity ratio we derive a bolometric correction $L(\mathrm{PAH\ 11.3\ \mu m})/L(\mathrm{bol}) = 0.0014$ from the spectrum (Sturm et al. 2000) and total far-infrared luminosity of M82 (Soifer et al. 1987). This correction factor is uncertain by at least a factor of 2, and depends critically on the amount of additional extinction of the PAH spectrum (above that suffered in M82) in the circumnuclear environments of these sources. To decrease the ratio $L(\mathrm{PAH\ 11.3\ \mu m})/L(\mathrm{bol})$ by an order of magnitude from that observed in M82 as a result of silicate absorption would require for the extinction curve of Li & Draine (2001) an additional overlying silicate optical depth at 9.7 μm of 3.8, or $A_V = 45$ mag above that affecting the M82 spectrum.

We have estimated the strength of the extended PAH emission (1) coincident with the continuum source and (2) integrated over the full extent of the PAH emission. We first measured the strength of the PAH band at a position adjacent to the continuum sources of Figure 2. To derive the PAH strength over the continuum source, we extrapolated this value to the spatial location of the continuum source. To determine the total PAH-emitting luminosity we integrated the flux in the PAH band over its visible area in the two-dimensional spectra of Figure 2. The PAH-band strengths (as measured above) were scaled to the measured fluxes of the continuum sources (matching bandpasses and spatial locations) from the imaging studies of these objects (Soifer et al. 1999, 2000, 2001). The uncertainty in converting PAH emission to flux is at least 30%, due to uncertainties in the location of the object in the slit.

The results of these estimates for the luminosity corresponding to the PAH emission are given in Table 3 for Arp 220 E, Arp 220 W, VV 114E$_{\mathrm{NE}}$, and Mrk 273N. The luminosities attributed to PAH-generating sources, i.e., circumnuclear starbursts, lie in the range from a few percent of the total bolometric luminosity in the Arp 220 sources to more than half the total luminosity in the compact source in VV 114E$_{\mathrm{NE}}$.

If the bolometric correction that we have adopted based on the PAH emission in M82 is an underestimate because of lower extinction to the PAH-emitting region in M82 than is appropriate for these galaxies, the circumnuclear luminosities associated with extended PAH emission in these systems

TABLE 3
LUMINOSITIES OF PAH-EMITTING REGIONS

Object	L_{bol}(cont)[a]	L_{bol}(PAH)[b,c] ($10^{10} \times L_{\odot}$)	L_{bol}(PAH)[c,d]
VV 114E$_{NE}$	5	2.5	12
VV 114E$_{SW}$	12	<1.2	...
IRAS 08572+3915	150	<15	...
Mrk 273NE	110	7	14
Mrk 273SW	25	<4	...
Mrk 463E	110	<11	...
Arp 220W	120	2	6[e]
Arp 220E	30	2	6[e]

[a] Continuum luminosities from Soifer et al. 1999, 2000, 2001.
[b] Bolometric luminosities from diffuse PAH emission overlying compact source, determined from the strength of the extended PAH band and applying the bolometric correction appropriate to M82 as described in the text. The uncertainty in this bolometric correction is at least a factor of 2.
[c] The luminosity cited here should be considered a lower limit because no correction has been applied for extinction to the PAH region beyond that suffered in the M82 spectrum.
[d] Total PAH-based bolometric luminosity from total 11.3 μm PAH emission as measured in two-dimensional spectrum of Fig. 2.
[e] Total PAH luminosity is measured for the extended region associated with both nuclei, Arp 220E and Apr 220 W.

would increase accordingly. In the case in which the PAH-to-bolometric luminosity ratio is $\sim 10^{-4}$, i.e., corresponding to $A_V \sim 50$ mag more than to M82, the extended PAH-emitting regions could account for roughly half the total bolometric luminosity of the sources. As discussed above for Arp 220, this seems extreme, since the continuum sources clearly dominate the mid-infrared flux in these observations and presumably dominate the far-infrared continuum as well.

5.4. *Mid-Infrared Spectra as Diagnostics of What Powers Compact Sources*

The spectra of the compact sources corrected for overlying PAH emission show a wide range of silicate optical depths, from $\sim$1 to $\sim$15, and PAH strengths ranging from no detectable PAH bands to modest PAH bands. Where the detectable silicate absorptions are small, i.e., Mrk 463E, Mrk 273SW, and VV 114E$_{SW}$, there is at most only weak evidence for PAH emission and in two of these cases strong evidence from optical spectroscopy for nonstellar (AGN) ionizing sources dominating the luminosity (Koski 1978; Miller & Goodrich 1990). In the other sources for which silicate absorption is much greater, there is at best only weak PAH emission in the mid-infrared specta.

Table 4 compiles the spectral classifications of these systems from a variety of wavelength regions. The last column of Table 4, from this work, is based on the strength of the 11.3 μm PAH band in the spectrum. The change in classification when correcting for the overlying PAH emission shows the importance of utilizing the highest possible spatial resolution.

Interpreting the mid-infrared spectra in terms of underlying sources is difficult at best. The present observations demonstrate again that the central regions of ULIRGs are quite complex. Continuum-emitting regions obscured by many tens of magnitudes of extinction and less obscured diffuse PAH-emitting regions fall within the central few hundred parsecs of these sources. Resolving these components in the mid-infrared requires the high spatial resolution afforded by the largest ground-based telescopes.

In the majority of nuclei, the 10 μm optical depth to the continuum sources is very large, so it is difficult to infer the nature of the underlying power source. The circumnuclear luminosities that can be attributed to star-

TABLE 4
SPECTRAL CLASSIFICATIONS OF COMPACT NUCLEI

Object	Spectral Class				
	Optical	Near IR	Mid-IR/*ISO*	X-Ray	Keck Mid-IR[a]
VV 114E$_{NE}$	H II[b]	SB[c]	AGN[d]	...	SB $\rightarrow$?
VV 114E$_{SW}$	H II[b]	SB[c]	AGN[d]	...	SB?
IRAS 08572+3915	LINER[b]	SB[e]	...	SB[f]	AGN
Mrk 273NE	Sey2[g]	SB[h]	AGN[i]	AGN[j,k]	SB $\rightarrow$?
Mrk 273SW	Sey2[g]	SB[h]	AGN[i]	AGN[j,k]	AGN?
Mrk 463E	Sey1[l]	...	...	AGN[m]	AGN
Arp 220E	LINER[b]	SB[h]	SB[i]	SB?[j]	SB $\rightarrow$?
Arp 220W	LINER[b]	SB[h]	SB[i]	SB?[j]	SB $\rightarrow$?

NOTE.— (SB) PAH feature clearly visible; (SB?) PAH feature marginally visible; (AGN) PAH feature not detected.
[a] Classifications are from strength of PAH band at 11.3 μm. First entry is from spectrum of Fig. 1; second entry (where appropriate) is from spectrum of Fig. 3.
[b] Veilleux et al. 1995.
[c] Doyon et al. 1995.
[d] Laurent et al. 2000.
[e] Murphy et al. 2001.
[f] Risaliti et al. 2000.
[g] Koski 1978.
[h] Goldader et al. 1995.
[i] Genzel et al. 1998.
[j] Iwasawa 1999.
[k] Xia et al. 2002.
[l] Miller & Goodrich 1990.
[m] Ueno et al. 1996.

bursts, from the diffuse PAH emission, are substantial and further highlight the picture of heavily dust- and gas-enshrouded environments, powered by a highly obscured source, with an overlying substantial starburst region that significantly affects the emergent spectra. The extent of the circumnuclear starburst region, as determined from the spatial extent of the PAH emission, is in the range 100–500 pc, a size that is resolvable at mid-infrared wavelengths only in the closest of these systems and only by the largest telescopes. From the spectra presented here, the large optical depths to the compact 10 μm sources suggest that even at these wavelengths the opacities are too large to probe the true centers of these regions. Whether the longer wavelength diagnostics of *SIRTF* or *HERSCHEL*, with their comparatively poor spatial resolution, can probe the cores of these systems is unclear.

We thank J. Aycock and R. Campbell for assistance with the observations and Barbara Jones, Rick Puetter, and the Keck team that brought the LWS into service, enabling these observations. S. Lord kindly provided the atmospheric model that was used to establish the wavelength calibration. G. Helou and L. Armus kindly read a draft of this manuscript. We thank the anonymous referee for providing helpful comments.

The W. M. Keck Observatory is operated as a scientific partnership between the California Institute of Technology, the University of California and the National Aeronautics and Space Administration. It was made possible by the generous financial support of the W. M. Keck Foundation. We extend special thanks to those of Hawaiian ancestry on whose sacred mountain we are privileged to be guests. Without their generous hospitality, none of the observations presented herein would have been possible. This research has made use of the NASA/IPAC Extragalactic Database, which is operated by the Jet Propulsion Laboratory, Caltech under contract with NASA.

B. T. S., K. M., and E. E. are supported by grants from the NSF and NASA. SIRTF is carried out at the Jet Propulsion Laboratory. A. J. W. was supported by NASA grant NAG 5-3042.

REFERENCES

Blain, A. W., Smail, I., Ivison, R. J., & Kneib, J.-P. 1999, MNRAS, 302, 632
Downs, D., & Solomon, P. M. 1998, ApJ, 507, 615
Doyon, R., Nadeau, D., Joseph, R. D., Goldader, J. D., Sanders, D. B., & Rowland, N. 1995, ApJ, 450, 111
Draine, B. T., & Anderson, N. 1985, ApJ, 292, 494
Dudley, C. C. 1999, MNRAS, 307, 553
Dudley, C. C., & Wynn-Williams, G. C. 1997, ApJ, 488, 720
Eales, S., Lilly, S., Webb, T., Dunne, L., Gear, W., Clements, D., & Yin, M. 2000, AJ, 120, 2244
Genzel, R., et al. 1998, ApJ, 498, 579
Gillett, F. C., Forrest, W. J., Merrill, K. M., Capps, R. W., & Soifer, B. T. 1975a, ApJ, 200, 609
Gillett, F. C., Kleinmann, D. E., Wright, E. L., & Capps, R. W. 1975b, ApJ, 198, L65
Goldader, J. D., Joseph, R. D., Doyon, R. D., & Sanders, D. B. 1995, ApJ, 444, 97
Hauser, M. G., & Dwek, E. 2001, ARA&A, 39, 249
Helou, G., Lu, N. Y., Werner, M. W., Malhotra, S., & Silbermann, N. 2000, ApJ, 532, L21
Iwasawa, K. 1999, MNRAS, 302, 96
Jones, B., & Puetter, R. C. 1993, Proc. SPIE, 1946, 610
Knop, R. A., Soifer, B. T., Graham, J. R., Matthews, K., Sanders, D. B., & Scoville, N. Z. 1994, AJ, 107, 920
Koski, A. T. 1978, ApJ, 223, 56
Larkin, J. E., Armus, L., Knop, R. A., Matthews, K., & Soifer, B. T. 1995, ApJ, 452, 599
Laurent, O., Mirabel, I. F., Charamandaris, V., Gallis, P., Madden, S. C., Sauvage, M., Vigroux, L., & Cesarsky, C. 2000, A&A, 359, 887
Leger, A., D'Hendecourt, L., & Defourneau, D. 1989, A&A, 216, 148
Li, A., & Draine, B. T. 2001, ApJ, 554, 778
Lord, S. 1992, NASA Tech. Mem. 103957
Lutz, D., Spoon, W. W., Rigopoulou, D., Moorwood, A. F. M., & Genzel, R. 1998, ApJ, 505, L103
Lutz, D., Sturm, E., Genzel, R., Moorwood, A., Alexander, T., Netzer, H., & Sternberg, A. 2000, ApJ, 536, 697
Mathis, J. S. 1990, ARA&A, 28, 37
Miller, J., & Goodrich, R. W. 1990, ApJ, 355, 456
Murphy, T. W., Soifer, B. T., Matthews, K., Armus, L., & Kiger, J. R. 2001, AJ, 121, 97
Myers, S. T., & Scoville, N. Z. 1987, ApJ, 312, L39
Rigopoulou, D., Spoon, H. W. W., Genzel, R., Lutz, D., Moorwood, A. F. M., & Tran, Q. D. 1999, AJ, 118, 2625
Risaliti, G., Gilli, R., Maiolino, R., & Salvati, M. 2000, A&A, 357, 13
Roche, P. F., Aitken, D. K., Smith, C. H., & Ward, M. J. 1991, MNRAS, 248, 606
Sakamoto, K., Scoville, N. Z., Yun, M. S., Crosas, M., Genzel, R., & Tacconi, L. J. 1999, ApJ, 514, 68
Sanders, D. B., Soifer, B. T., Elias, J. H., Madore, B. F., Matthews, K., Neugebauer, G., & Scoville, N. Z. 1988a, ApJ, 325, 74
Sanders, D. B., Soifer, B. T., Elias, J. H., Neugebauer, G., & Matthews, K. 1988b, ApJ, 328, L35
Scoville, N. Z., et al. 2000, AJ, 119, 991
Sellgren, K. 1984, ApJ, 277, 623
Smith, C. H., Aitken, D. K., & Roche, P. K. 1989, MNRAS, 241, 425
Soifer, B. T., et al. 1984, ApJ, 283, L1
Soifer, B. T., Neugebauer, G., Matthews, K., Becklin, E. E., Ressler, M., Werner, M. W., Weinberger, A. J., & Egami, E. 1999, ApJ, 513, 207
Soifer, B. T., et al. 2000, AJ, 119, 509
———. 2001, AJ, 122, 1213
Soifer, B. T., Sanders, D. B., Madore, B. F., Neugebauer, G., Danielson, G. E., Elias, J. H., Lonsdale, C. J., & Rice, W. L. 1987, ApJ, 320, 238
Sturm, E., Alexander, T., Lutz, D., Sternberg, A., Netzer, H., & Genzel, R. 1999, ApJ, 512, 197
Sturm, E., et al. 1996, A&A, 315, L133
Sturm, E., Lutz, D., Tran, D., Feuchtgruber, H., Genzel, R., Kunze, D., Moorwood, A. F. M., & Thornley, M. D. 2000, A&A, 358, 481
Tran, Q. D., et al. 2001, ApJ, 552, 527
Ueno, S., Koyama, K., Awaki, H., Hayashi, I., & Blanco, P. R. 1996, PASJ, 48, 389
Veilleux, S., Kim, D.-C., Sanders, D. B., Mazzarella, J. M., & Soifer, B. T. 1995, ApJS, 98, 171
Willner, S. P., Soifer, B. T., Russell, R. W., Joyce, R., & Gillett, F. C. 1977, ApJ, 217, L121
Wilson, A. S., Helfer, T. T., Haniff, C. A., & Ward, M. J. 1991, ApJ, 381, 79
Xia, X. Y., Xue, S. J., Mao, S., Boller, Th., Deng, Z. G., & Wu, H. 2002, ApJ, 564, 196